Nanoscale

PAPER

View Article Online
View Journal | View Issue

Cite this: *Nanoscale*, 2020, **12**, 23824

Electrochemically controlled cleavage of imine bonds on a graphene platform: towards new electro-responsive hybrids for drug release†

Hui-Lei Hou, [a] Lucia Cardo, [a] Donato Mancino, [a] Blanca Arnaiz, [a] Alejandro Criado *[a] and Maurizio Prato *[a,b,c]

Received 28th May 2020,
Accepted 4th August 2020

DOI: 10.1039/d0nr04102e

rsc.li/nanoscale

Graphene-based materials are particularly suitable platforms for the development of new systems able to release drugs upon the application of controlled electrochemical stimuli. Herein, we report a new electro-responsive graphene carrier functionalised with aldehydes (as drug models) through imine-based linkers. We explore a new type of drug loading/release combination based on the formation of a covalent bond and its cleavage upon electrolysis. The new graphene–drug model hybrid is stable under physiological conditions and displays a fast drug release upon the application of low voltages.

The development of systems able to deliver therapeutics to specific biological targets and control their release is one major challenge in modern medicine. This possibility would enhance treatment efficiency, minimise possible related side effects and improve the compliance of single patients. In the last few decades, various strategies have been proposed, many of which are based on triggering the drug specificity and release by using endogenous environmental changes (*i.e.* pH changes, enzymatic activities, different redox settings naturally occurring in biological systems)[1–5] and/or as a response upon applying external stimuli, such as heat,[6,7] ultrasounds,[8,9] magnetic fields,[10,11] irradiation[12–14] or electrical modulation.[15–17] In most of these approaches, drugs are conjugated to biocompatible nanomaterials with different chemical and physical properties, selected depending on the type of drug, target site, release rate, dosage, and stimuli involved in the controlled drug release strategy.

Among the large variety of promising materials developed and investigated for this application, carbon-based nanomaterials, particularly 2D materials like graphene and its derivatives (*i.e.* graphene oxide (GO) and reduced graphene oxide (rGO)), have received much attention.[18–21] Similarly to many nanomaterials employed as bio-carriers, graphene-based materials (GBMs) can be easily modified with several functional groups,[22,23] allowing the design of different crosslinking strategies with synthetic agents and biomolecules, with controllable and high cargo-loading capacity and density; they are transparent in the visible range and potentially biocompatible and exhibit good cell adhesion. More exclusively, they are among the strongest and most stable materials available, although they possess high flexibility,[18–21] and they have excellent electron and thermal conductivity capabilities. Such a unique set of features in just one material is particularly strategic for bio-applications such as bio-sensing,[24,25] tissue engineering,[26] bio-electronics[25,27–30] and electronically and/or photo/thermal induced drug/gene delivery.[20,31–33]

Electrochemical control of drug release is a very attractive strategy in drug delivery, because the drug release is induced by electrical external stimuli that are relatively easy to generate and control, possibly using size-reduced devices, with high sensitivity and the potential ability to be controlled remotely.[15–17,34] At the same time, graphene-based materials are potentially ideal platforms for this purpose, not only for their remarkable conductivity properties able to record electrical activity in living cells with high sensitivity,[29] but also for their electrochemical inertness and flexibility that allow their integration into biocompatible micro-devices suitable for *in vivo* applications.[30,35]

Because of the delocalised π electrons on the surface of graphene, a very common method to develop graphene–drug systems consists of directly absorbing aromatic agents (often water insoluble drugs) onto graphene platforms by π–π stacking and other non-covalent interactions. However, for an electro-responsive type of release, this strategy often does not allow a fine control of drug dosage in real time and limits the type of drug that can be employed. Alternatively graphene/bio-

[a]*Center for Cooperative Research in Biomaterials (CIC biomaGUNE), Basque Research and Technology Alliance (BRTA), Paseo de Miramón 182, 20014 Donostia San Sebastián, Spain. E-mail: acriado@cicbiomagune.es, prato@units.it*
[b]*Department of Chemical and Pharmaceutical Sciences, Università degli Studi di Trieste, Via Licio Giorgieri 1, Trieste 34127, Italy*
[c]*Basque Foundation for Science, Ikerbasque, Bilbao 48013, Spain*

† Electronic supplementary information (ESI) available: Experimental details and ESI figures. See DOI: 10.1039/d0nr04102e

compatible polymer hybrids are employed to "wrap" or "trap" the active agent; thus, a finer regulation of the release is possible, but this might require highly positive voltages (>10 V) and/or long stimuli time (>30 min).[36–39] Given the potential of graphene for this application and bio-electronics in general, there is a real need to investigate alternative drug coating/release combinations to enhance the versatility and efficiency of graphene-based supports.

Herein, we designed an electro-responsive hybrid of graphene conjugated with drug models by using a covalent-bond-based linker. In more detail, a support of exfoliated graphene is first functionalised with aniline groups (f-G(**1**) in Scheme 1a) followed by conjugation with two different types of drug models containing aldehyde groups and achieving two hybrid systems in which potential drugs are covalently anchored *via* an imine bond (f-G(**2**) and f-G(**3**) in Scheme 1a). We conjugated *via* Schiff bases because these groups are known to undertake irreversible electrochemical oxidation under low voltage conditions;[40–42] hence, they are potentially ideal cleavable linkers for electro-responsive drug triggering. We anticipate the release of the aldehyde-drug upon electrolysis and, according to the literature,[43,44] we hypothesise f-G(**4**) as a graphene residue. To the best of our knowledge, the use of modified graphene for the electrically controlled release of a covalently attached drug has not been reported yet.

To characterise drug loading and release of our designed system, we selected two different aldehydes, 9-anthracenecarboxaldehyde (**3**) and pentafluorobenzaldehyde (**4**) (Scheme 1), as models that are easy to monitor by optical and X-ray photoelectron spectroscopy (XPS), respectively. However, we first evaluated the suitability of the electro-responsive cleavable linker only, by selecting and characterising the graphene-free system *N*-(anthracen-9-ylmethylene)-4-methylaniline (**5**) (Scheme 1b) as an analogue of f-G(**2**).

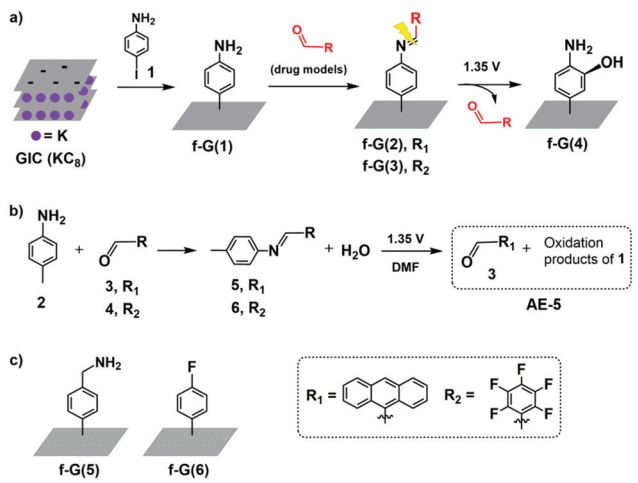

Scheme 1 Schematics of the preparation of (a) the graphene-based platform f-G(**1**) loaded with the drug models (f-G(**2**–**3**)) followed by their electrochemically triggered release (f-G(**4**)); (b) graphene-free organic models employed to characterise the release mechanism; (c) graphene-based materials for the control experiments.

The electrolysis of **5** was performed in DMF at 1.35 V *vs.* Ag/AgCl (see the ESI† for details), yielding the mixture **AE-5** (Scheme 1b), expected to contain the released aldehyde **3** and additional oxidation products. Water was added to the mixture after the electrolysis and the resulting precipitate was analysed by ^{1}H NMR, showing indeed the presence of **3** as the main product (Fig. 1a, bottom trace). Whilst this procedure allowed the extraction of pure **3**, we also performed electrolysis in

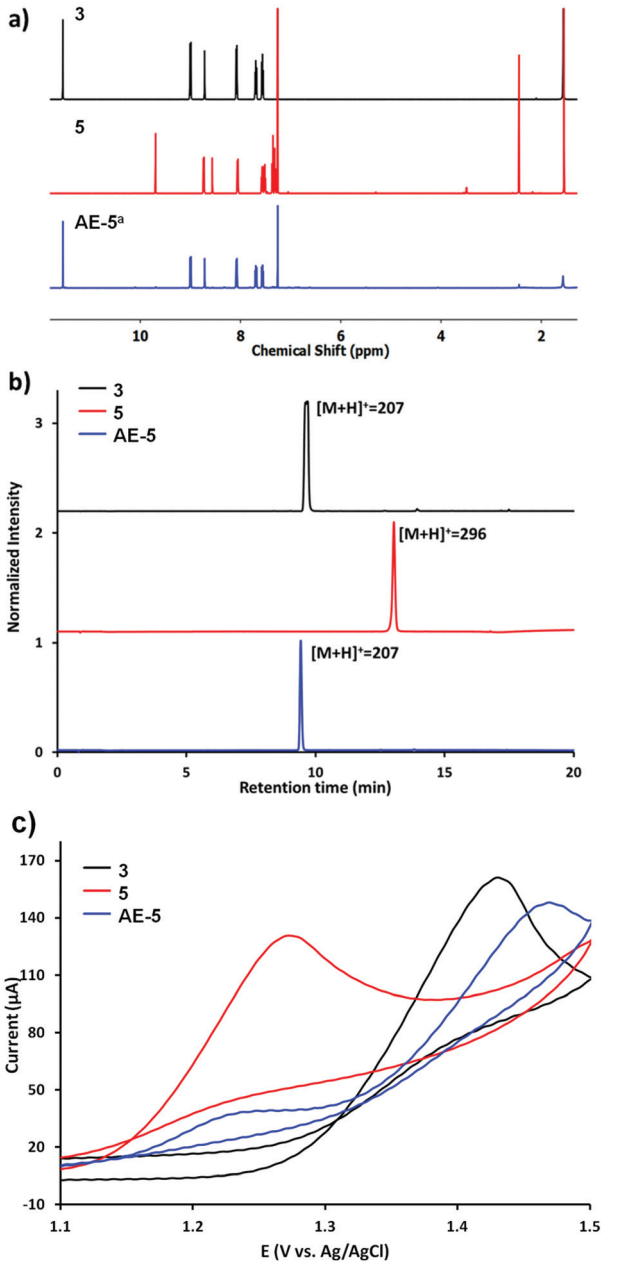

Fig. 1 (a) ^{1}H NMR (CD3Cl, 500 MHz) of compounds **3** and **5** before electrolysis (top and middle trace, respectively) and **AE-5**[a] (the **AE-5** mixture after electrolysis followed by precipitation with water, bottom trace); (b) UPLC traces of **3** and **5** before electrolysis (top and middle, respectively) and the **AE-5** mixture after electrolysis and dilution in acetonitrile (detection at 403 nm); (c) CV of **3** (black line) and **5** (red line) before electrolysis and the **AE-5** mixture (blue line) after electrolysis.

DMF-d_7 (under the same concentration and voltage conditions) and analysed the crude product of the reaction **AE-5** without further manipulation: again, the ^{1}H NMR spectrum showed the presence of **3** as the main product of the reaction (Fig. S10 and S11†), whilst the starting material **5** (analysed as a control) was stable in the same solvent and reaction time (Fig. S12†), confirming that the cleavage of aldehyde **3** occurs only as a result of the electrolysis process and unwanted hydrolysis effects were not observed in this system.

The mixture **AE-5** was also compared with starting materials **3** and **5** by ultra-performance liquid chromatography-mass spectrometry (UPLC-MS). The chromatogram of the mixture shows one prevalent peak with the retention time and mass equivalent to those of the starting aldehyde **3** (Fig. 1b). Cyclic voltammetries (CVs) of **AE-5** compared with those of **3** and **5** (as references) are shown in Fig. 1c and S8.† The CV of **5** (red line) presents an irreversible oxidation peak at 1.27 V *vs.* Ag/AgCl, indicating that it decomposes upon electrooxidation. The further increase of the current at 1.4–1.5 V is due to the oxidation of the anthracene moiety as shown by the CV of **3** (black line). The cyclic voltammogram of the **AE-5** (blue line) mixture shows a decrease of the peak related to the oxidation of **5** (1.28 V) and the presence of a new strong peak at 1.48 V most probably due to the oxidation of **3**, although the shift of the peak compared to that of **3** alone confirmed the presence of other products in the mixture. This result suggests that **5** was significantly reduced after electrolysis, and **3** was the main product. The UV-vis profile and the ^{1}H NMR spectrum of **AE-5** (Fig. S9 and S11,† respectively) are consistent with the presence of **3** in the mixture. In addition, the ^{1}H NMR spectrum of the crude product **AE-5** did not show any detectable side-products, so we can assume that no soluble compounds derived from the oxidation of aniline were obtained.[45] We finally checked the stability of the imine linker of **3**, as imine bonds are known to be unstable in aqueous media or even in organic solvents containing traces of water, although their hydrolysis can be inhibited by steric hindrance.[46] The ^{1}H NMR analysis of **5** before and after three days of incubation in the serum shows no changes (Fig. S6 and S7†).

Overall, the first control experiments using the graphene free analogues **5** confirmed the stability of the imine linker under cell biology experimental conditions and the efficient cleavage of the imine bond upon electrolysis, yielding the free aldehyde-drug **3**, similarly to the reported electrochemical oxidation of aliphatic amines.[44] The presence of additional complex oxidation products from *p*-toluidine are expected upon electrolysis. Different attempts to characterise (by NMR, mass spectrometry and HPLC) these side products failed. However, we suggest the presence of polyanilines derived from the *ortho*-coupling process of *p*-toluidine derivatives.[45]

With this information in hand, we transferred the investigation to the graphene-based system. *p*-Aniline functionalised graphene f-G(**1**) was obtained by the reaction of a graphite intercalation compound (GIC) with 4-iodoaniline (**1**) (Scheme 1a and the ESI† for details).[47] The successful covalent functionalisation of graphene was confirmed by scanning Raman spectroscopy (SRS). I_D/I_G, which is related to the degree of covalent functionalisation, increased from 0.71 for the control experiment (CE) to 0.98 for f-G(**1**) (Fig. S17†). In order to quantify the amount of disorder, the distance between 0D-point like defects (L_D) was calculated from the Raman spectroscopic data (eqn (S1)†).[48] Considering the CE as non-chemically modified graphene, f-G(**1**) showed an average distance of 23 nm between the electro-grafted groups, which confirms a moderate functionalization. This finding is in line with the estimated functionalization degree determined from TGA profiles (Table S6 and Fig. S19†). Furthermore, nitrogen introduced upon functionalization with aniline was detected by XPS in f-G(**1**) (N atom concentration 1%, Table S1†). The Kaiser test (KT)[49] is usually employed to quantify amino groups attached to nanomaterials but it requires the presence of aliphatic primary amines; therefore, we performed the KT using f-G(**5**) (Schemes 1c and S6, and Table S5†) as an analogue of f-G(**1**) in which graphene is functionalized with a benzyl amine. The KT confirmed the presence of a primary amine in f-G(**5**) at a concentration of 24 μmol g^{-1} (Fig. S18†). It is worth mentioning that f-G(**5**) was not selected as part of the delivery platform because of the known instability of the bond between methylene and nitrogen atom of benzyl amine groups under electrolytic conditions.[44]

Aldehydes **3** and **4** were anchored on f-G(**1**) by an imine bond to afford f-G(**2** and **3**) (Scheme 1). The drug release of f-G (**2**) upon electrochemical oxidation was monitored by fluorescence spectrophotometry (Fig. 2). No fluorescence signal was detected upon washing the eluents before the electrolysis of f-G(**2**) (black line), confirming the absence of the unbound drug in the system. But the eluent analysed after the electrolysis showed a strong emission profile (blue line) analogous to the emission of **3** (red line as a control), confirming the release of the drug from f-G(**2**). This oxidation reaction probably occurs by one electron transfer reaction by the formation of a radical cation.[40] To ensure that only imine bonds are

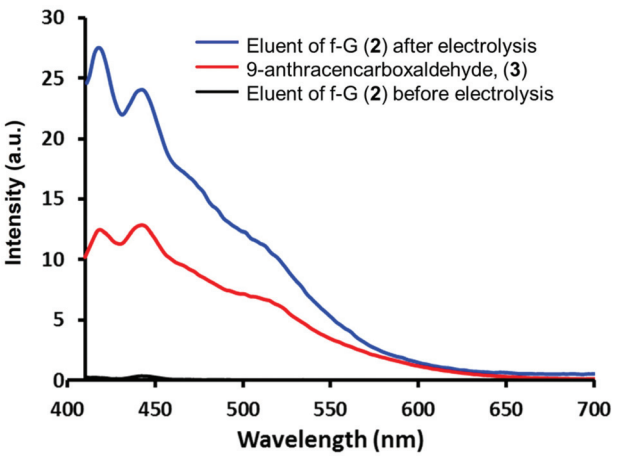

Fig. 2 Fluorescence emission spectra of 9-anthracenecarboxaldehyde (**3**) and the eluent before and after the electrolysis of f-G(**2**) in DMF.

cleaved during electrochemical oxidation whilst the phenyl group remains attached to the graphene structure, we performed the same electrolysis experiment using f-G(**6**) (Scheme S7 and Table S2†), where fluorobenzene is covalently bonded to graphene, and additional fluorine atoms are easily quantified by XPS analysis. Comparable percentages of fluorine were detected by XPS before and after applying 1.35 V (2.8% *vs.* 2.9%, respectively). This proves that the C–C bond between graphene and the phenyl group is stable under the electrolysis conditions applied and the released anthracenyl moiety detected in Fig. 2 belongs to the free aldehyde upon the cleavage of the imine bond. In order to study the effect of possible pi–pi adsorption of aromatic molecules on modified graphene, a control experiment based on f-G(**1**) treated with anthracene was performed (Scheme S8†). The resulting graphene material f-G(**1**)* was analysed by TGA and compared with f-G(**1**) and f-G(**2**), showing a low functional degree of 29 μmol g^{-1} with respect to anthracene. However, after the electrolysis of f-G(**1**)*, a rather weak fluorescent signal of non-covalently adsorbed aromatic anthracene was detected, with a very low intensity when compared to the signal of the anthracene derivative detected upon the electrolysis of f-G(**2**) (Fig. S20†); this confirms that a minor yet possible non-covalent absorption of the aromatic drug model on graphene does not significantly interfere with the desired drug release effect. In order to study the effect of possible pi–pi adsorption of aromatic molecules on exfoliated graphene, a control experiment based on the CE treated with **3** was performed (Scheme S7†). Then the electrolysis of the resulting graphene material CE* was performed and compared with f-G(**2**). A rather weak fluorescent signal of non-covalently adsorbed aromatic **3** was detected after the electrolysis of CE*, with a very low intensity when compared to the signal of **3** detected upon the electrolysis of f-G(**2**) (Fig. S20†); this confirms that a minor yet possible non-covalent absorption of the aromatic drug model on graphene does not significantly interfere with the desired drug release effect.

Quantitative analysis of drug loading and release was performed using our second model f-G(**3**), taking advantage of the measurements of the fluorine percentage by XPS. Drug model **6** (4-methyl-*N*-(perfluorobenzylidene)aniline in Schemes 1b and S2†)[50] was used as a reference of a "graphene-free" analogue of f-G(**3**). Then a home-made working electrode was manufactured by pasting f-G(**3**) on an ITO electrode with conductive copper tape to simulate a chip of a possible bio-device (Fig. S21†). The atomic concentration of each element in f-G(**3**), measured by XPS, is presented in Table S3,† and the loading percentage *L*% of drug **4** was 41%, calculated with respect to nitrogen, using the following eqn (1):

$$L\% = \frac{\mathrm{At(F)}}{5 \times \mathrm{At(N)}} \times 100\% \quad (1)$$

where At(F) and At(N) are the atomic concentrations of fluorine and nitrogen in f-G(**3**), respectively.

The residue of f-G(**3**) after electrochemical oxidation was also analysed by XPS and the percentage of the released **4** (*R*%) from f-G(**3**) was calculated using the following eqn (2):

$$R\% = \frac{L(\mathrm{BE}) - L(\mathrm{AE})}{L(\mathrm{BE})} \times 100\% \quad (2)$$

where *L*(BE) and *L*(AE) are the loading percentages of **4** before and after the electrolysis of f-G(**3**), respectively.

As shown in Fig. 3, electro-oxidation induces 43% of the burst drug release during the first 10 s followed by a more sustained release (62% in 120 s; see the ESI† for details). Importantly, without the application of the potential, the release of aldehyde was only 9.5% in 120 s, which confirms the accelerated aldehyde release under the applied voltage. Such a rapid drug release is a very desired feature when developing carrier–drug hybrids, particularly because it helps to overcome drug resistance.[51] Note that the SEM images of deposited f-G (**3**) in the electrode (Fig. S22†) showed a surface composed of different stacked graphene structures. Thus, it is reasonable that the obtained non-complete release (62%) of the drug after electro-oxidation is due to the morphology of the electrode surface and trapped molecules between layers. Additionally, SEM images showed an apparent thickness of ~1 mm for an individual f-G(**3**) structure, which evidences the typical multilayer structure of chemically exfoliated graphene.

According to the tendency of the previously reported electrochemical oxidation of *para*-toluidines towards the *ortho*-coupling process,[45] we hypothesise the aminophenol-substituted f-G(**4**) in Scheme 1a as a possible product of electrolysis. Hence, f-G(**4**) would be obtained by the addition of the hydroxyl groups present in the media (trace of water in DMF) in the *ortho*-position of the phenyl ring. The increment of the atomic concentration of oxygen of f-G(**4**) with respect to f-G(**1**) (Tables S1 and S4†) obtained by XPS supports our hypothesis.

The properties displayed by graphene place this 2D material among the most attractive and versatile materials for a large number of applications; therefore any issue concerning their safety is crucial for any application (not only bio-medical

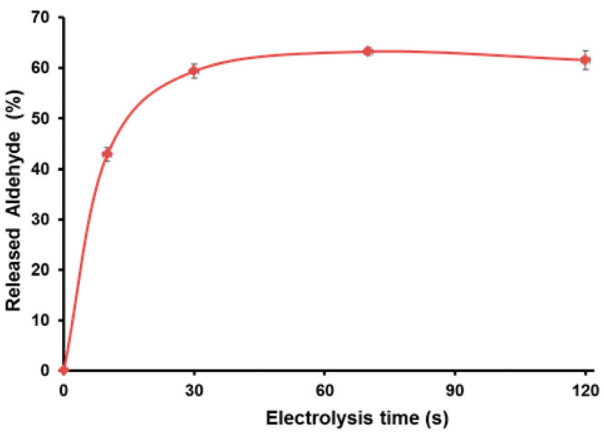

Fig. 3 (a) Cumulative release profile of the aldehyde from f-G(**3**) at 1.35 V *vs.* Ag/AgCl, and each time point was repeated three times.

related) and a possible obstacle for translation to the industry. Studies performed in the last decade show that the toxicity in different biological systems strongly depends on the size, shape, surface properties, and functionalization/passivation methods of the graphene platform and certainly indicates that safety needs to be assessed for any newly proposed graphene-based material.[18,52–54] We performed cell viability assays (by the MTS test[55]) using the mouse astrocyte cell line C8-D1A in the presence of our graphene-based carriers, CE (graphene support before functionalisation with aniline) and f-G(**1**), at different concentrations for 24 and 72 h. The cell viability remained above 80% even at the highest concentration tested (100 μg mL^{-1}, Fig. S5†) and this further indicates the potential suitability of this graphene platform for bio-applications. The next step for this study will focus on exploring the electrically controlled release of different drugs toward specific biological targets.

In conclusion, an electrochemically controlled delivery system was fabricated by covalently binding aldehydes (**3** and **4**) to a graphene platform pre-coated with aniline groups (f-G (**1**)) to form imine bonds. The aldehydes used as drug models were responsively released from the graphene platform upon the cleavage of the imine linker induced by electro-oxidation at a relatively low voltage (1.35 V *vs.* Ag/AgCl) compared to some reported studies.[36–38] The carrier–drug system is relatively stable under the conditions employed (graphene losing only 9.5% of the attached aldehyde), whilst 40% of the cargo is released during the first 10 s upon the application of the voltage, achieving a total release of 60% in 60 s.

Thus the system developed here displays fast, time-depending and electro-responsive release of the cargo from its support, and preliminary studies in cells confirm the potential biocompatibility of the material employed, which are the key features in the design of hybrids for electro-controlled drug release. Importantly, here we focused on establishing a novel approach to coat an electro-responsive graphene support with drug models, focusing on employing a covalent bond between the cargo and the graphene carrier, rather than depending on π–π and non-covalent interactions. This new strategy potentially offers a better control and characterisation of the loading as well as the release of the drug upon the application of electro-stimuli, and introduces the use of electro-responsive graphene as a support not only for aromatic agents but also for smaller or non-aromatic drugs and other functional agents. Given the high potential of the hybrid developed, we are now focusing on complementary studies useful to design a controllable drug release system compatible for *in vivo* studies. In particular, the approach developed here will be implemented by exploring alternative graphene derivatives such as CVD graphene or graphene oxide, which recently showed impressive potential as electro-responsive components of implantable devices, with abilities to either record electrical activity (*i.e.* within neuronal interfaces) or perform electrochemical stimulation *in vivo*.[27,30,35] At the same time we are already exploring different biologically significant cargos (*i.e.* drugs), combined with different cargo/graphene loading and electrochemical stimulation time/power conditions, to identify the best options and optimize a fine ON/OFF control of cargo release.

Conflicts of interest

There are no conflicts to declare.

Acknowledgements

M. Prato is the recipient of the AXA Chair (2016–2023). A. Criado, H.-L. Hou and D. Mancino thank MINECO for their research grants (Juan de la Cierva – Incorporación No. IJCI-2016-31113 and IJC-2018-037396 for A. Criado and H.-L. Hou, respectively; and FPI No. BES-2017-081563 for D. Mancino). This work was supported by the Graphene Flagship Core 2 and Core 3 grant agreement (No. 785219 and 881603, respectively) and EU H2020-MSCA-RISE-2016 (No. 734381). This work was performed under the Maria de Maeztu Units of Excellence Program from the Spanish State Research Agency – Grant No. MDM-2017-0720.

Notes and references

1 Z. Ge and S. Liu, Functional block copolymer assemblies responsive to tumor and intracellular microenvironments for site-specific drug delivery and enhanced imaging performance, *Chem. Soc. Rev.*, 2013, **42**, 7289–7325.
2 L. Bruelisauer, M. A. Gauthier and J.-C. Leroux, Disulfide-containing parenteral delivery systems and their redox-biological fate, *J. Controlled Release*, 2014, **195**, 147–154.
3 R. Tong, *et al.*, Smart chemistry in polymeric nanomedicine, *Chem. Soc. Rev.*, 2014, **43**, 6982–7012.
4 R. Cheng, F. Meng, C. Deng and Z. Zhong, Bioresponsive polymeric nanotherapeutics for targeted cancer chemotherapy, *Nano Today*, 2015, **10**, 656–670.
5 N. Kamaly, B. Yameen, J. Wu and O. C. Farokhzad, Degradable Controlled-Release Polymers and Polymeric Nanoparticles: Mechanisms of Controlling Drug Release, *Chem. Rev.*, 2016, **116**, 2602–2663.
6 E. Carrasco, *et al.*, Intratumoral Thermal Reading During Photo-Thermal Therapy by Multifunctional Fluorescent Nanoparticles, *Adv. Funct. Mater.*, 2015, **25**, 615–626.
7 H. Chen, *et al.*, Combined chemo- and photo-thermal therapy delivered by multifunctional theranostic gold nanorod-loaded microcapsules, *Nanoscale*, 2015, **7**, 8884–8897.
8 J. J. Kwan, *et al.*, Ultrasound-Propelled Nanocups for Drug Delivery, *Small*, 2015, **11**, 5305–5314.
9 T. Boissenot, A. Bordat, E. Fattal and N. Tsapis, Ultrasound-triggered drug delivery for cancer treatment using drug delivery systems: From theoretical considerations to practical applications, *J. Controlled Release*, 2016, **241**, 144–163.

10 Y. Qiu, *et al.*, Magnetic forces enable controlled drug delivery by disrupting endothelial cell-cell junctions, *Nat. Commun.*, 2017, **8**, 15594.
11 Y. Namiki, *et al.*, A novel magnetic crystal-lipid nanostructure for magnetically guided in vivo gene delivery, *Nat. Nanotechnol.*, 2009, **4**, 598–606.
12 L. Zou, *et al.*, Current Approaches of Photothermal Therapy in Treating Cancer Metastasis with Nanotherapeutics, *Theranostics*, 2016, **6**, 762–772.
13 S. Alonso-de Castro, *et al.* Riboflavin as a bioorthogonal photocatalyst for the activation of a Pt-IV prodrug, *Chem. Sci.*, 2017, **8**, 4619–4625.
14 Y. Liu, P. Bhattarai, Z. Dai and X. Chen, Photothermal therapy and photoacoustic imaging via nanotheranostics in fighting cancer, *Chem. Soc. Rev.*, 2019, **48**, 2053–2108.
15 D. Samanta, R. Mehrotra, K. Margulis and R. N. Zare, On-demand electrically controlled drug release from resorbable nanocomposite films, *Nanoscale*, 2017, **9**, 16429–16436.
16 Y. Zhao, A. C. Tavares and M. A. Gauthier, Nano-engineered electro-responsive drug delivery systems, *J. Mater. Chem. B*, 2016, **4**, 3019–3030.
17 D. Uppalapati, B. J. Boyd, S. Garg, J. Travas-Sejdic and D. Svirskis, Conducting polymers with defined micro- or nanostructures for drug delivery, *Biomaterials*, 2016, **111**, 149–162.
18 C. Cheng, S. Li, A. Thomas, N. A. Kotov and R. Haag, Functional Graphene Nanomaterials Based Architectures: Biointeractions, Fabrications, and Emerging Biological Applications, *Chem. Rev.*, 2017, **117**, 1826–1914.
19 D. K. Ji, C. Ménard-Moyon and A. Bianco, Physically-triggered nanosystems based on two-dimensional materials for cancer theranostics, *Adv. Drug Delivery Rev.*, 2019, **138**, 211–232.
20 Z. Gu, S. Zhu, L. Yan, F. Zhao and Y. Zhao, Graphene-Based Smart Platforms for Combined Cancer Therapy, *Adv. Mater.*, 2019, **31**, 1800662.
21 G. Reina, *et al.*, Promises, facts and challenges for graphene in biomedical applications, *Chem. Soc. Rev.*, 2017, 4400–4416, DOI: 10.1039/C7CS00363C.
22 A. Criado, M. Melchionna, S. Marchesan and M. Prato, The Covalent Functionalization of Graphene on Substrates, *Angew. Chem., Int. Ed.*, 2015, **54**, 10734–10750.
23 M. Quintana, E. Vazquez and M. Prato, Organic functionalization of graphene in dispersions, *Acc. Chem. Res.*, 2013, **46**, 138–148.
24 L. Wang, Q. Xiong, F. Xiao and H. Duan, 2D nanomaterials based electrochemical biosensors for cancer diagnosis, *Biosens. Bioelectron.*, 2017, **89**, 136–151.
25 F. Veliev, *et al.*, Sensing ion channel in neuron networks with graphene field effect transistors, *2D Mater.*, 2018, **5**, 045020.
26 D. A. Jasim, *et al.*, Graphene-based papers as substrates for cell growth: Characterisation and impact on mammalian cells, *FlatChem*, 2018, **12**, 17–25.
27 K. Kostarelos, M. Vincent, C. Hebert and J. A. Garrido, Graphene in the Design and Engineering of Next-Generation Neural Interfaces, *Adv. Mater.*, 2017, **29**, 1700909.
28 L. H. Hess, M. Seifert and J. A. Garrido, Graphene transistors for bioelectronics, *Proc. IEEE*, 2013, **101**, 1780–1792.
29 B. M. Blaschke, *et al.*, Flexible graphene transistors for recording cell action potentials, *2D Mater.*, 2016, **3**, 025007.
30 E. Masvidal-Codina, *et al.*, High-resolution mapping of infraslow cortical brain activity enabled by graphene microtransistors, *Nat. Mater.*, 2019, **18**, 280–288.
31 Y. W. Chen, Y. L. Su, S. H. Hu and S. Y. Chen, Functionalized graphene nanocomposites for enhancing photothermal therapy in tumor treatment, *Adv. Drug Delivery Rev.*, 2016, **105**, 190–204.
32 H. Kim and W. J. Kim, Photothermally controlled gene delivery by reduced graphene oxide-polyethylenimine nanocomposite, *Small*, 2014, **10**, 117–126.
33 C. L. Weaver, J. M. Larosa, X. Luo and X. T. Cui, Electrically controlled drug delivery from graphene oxide nanocomposite films, *ACS Nano*, 2014, **8**, 1834–1843.
34 J. Kolosnjaj-Tabi, L. Gibot, I. Fourquaux, M. Golzio and M. P. Rols, Electric field-responsive nanoparticles and electric fields: physical, chemical, biological mechanisms and therapeutic prospects, *Adv. Drug Delivery Rev.*, 2019, **138**, 56–67.
35 B. M. Blaschke, *et al.*, Mapping brain activity with flexible graphene micro-transistors, *2D Mater.*, 2017, **4**, 025040.
36 A. Servant, *et al.* Graphene-based electroresponsive scaffolds as polymeric implants for on-demand drug delivery, *Adv. Healthcare Mater.*, 2014, **3**, 1334–1343.
37 H. W. Liu, S. H. Hu, Y. W. Chen and S. Y. Chen, Characterization and drug release behavior of highly responsive chip-like electrically modulated reduced graphene oxide-poly(vinyl alcohol) membranes, *J. Mater. Chem.*, 2012, **22**, 17311–17320.
38 N. Mac Kenna, P. Calvert, A. Morrin, G. G. Wallace and S. E. Moulton, Electro-stimulated release from a reduced graphene oxide composite hydrogel, *J. Mater. Chem. B*, 2015, **3**, 2530–2537.
39 S. Merino, C. Martín, K. Kostarelos, M. Prato and E. Vázquez, Nanocomposite hydrogels: 3D polymer-nanoparticle synergies for on-demand drug delivery, *ACS Nano*, 2015, **9**, 4686–4697.
40 T. Balić, B. Marković and M. Medvidović-Kosanović, Electrochemical and structural analysis of a novel symmetrical bis-Schiff base with herringbone packing motif, *J. Mol. Struct.*, 2015, **1084**, 82–88.
41 H. L. Hou, Z. J. Li, Y. Wang and X. Gao, Reductive benzylation of C60 imidazoline with a bulky addend, *Org. Lett.*, 2014, **16**, 712–715.
42 H. L. Hou, Z. J. Li, Y. Wang and X. Gao, Reductive benzylation of C70 imidazoline with a bulky addend, *J. Org. Chem.*, 2014, **79**, 8865–8870.
43 M. C. Carreño and M. Ribagorda, Anodic oxidation of N-protected 4-methoxy anilines: Improved synthesis of quinone imine acetals, *J. Org. Chem.*, 2000, **65**, 1231–1234.

44 A. Adenier, M. M. Chehimi, I. Gallardo, J. Pinson and N. Vilà, Electrochemical oxidation of aliphatic amines and their attachment to carbon and metal surfaces, *Langmuir*, 2004, **20**, 8243–8253.
45 P. G. Desideri, L. Lepri and D. Heimler, Electrochemical behavior of the toluidines in aqueous solution – part II. Para-Toluidine, *J. Electroanal. Chem. Interfacial Electrochem.*, 1974, **52**, 105–114.
46 S. Levinger, R. Nair and A. Hassner, The role of an aromatic group in remote chiral induction during conjugate addition of α-sulfonylallylic carbanions to ethyl crotonate, *Beilstein J. Org. Chem.*, 2008, **4**, 1–5.
47 H. Hou, J. P. Merino, A. Criado, A. Hirsch and M. Prato, The reactivity of reduced graphene depends on solvation, *2D Mater.*, 2019, **6**, 025009.
48 L. G. Cançado, *et al.*, Quantifying defects in graphene via Raman spectroscopy at different excitation energies, *Nano Lett.*, 2011, **11**, 3190–3196.
49 D. J. McCaldin, The Chemistry of Ninhydrin, *Chem. Rev.*, 1960, **60**, 39–51.
50 Y.-L. Zhou, X.-D. Jia, R. Li, B. Han and L.-M. Wu, Synthesis of furano [3,2-*c*]- and pyrano [3,2-*c*]quinolines upon imino Diels-Alder reactions initiated by nitrosonium (NO^+), *Chin. J. Chem.*, 2007, **25**, 422–425.
51 Q. Yin, J. Shen, Z. Zhang, H. Yu and Y. Li, Reversal of multidrug resistance by stimuli-responsive drug delivery systems for therapy of tumor, *Adv. Drug Delivery Rev.*, 2013, **65**, 1699–1715.
52 M. V. D. Z. Park, *et al.*, Considerations for Safe Innovation: The Case of Graphene, *ACS Nano*, 2017, **11**, 9574–9593.
53 C. Martín, K. Kostarelos, M. Prato and A. Bianco, Biocompatibility and biodegradability of 2D materials: Graphene and beyond, *Chem. Commun.*, 2019, **55**, 5540–5546.
54 B. Fadeel, *et al.*, Safety Assessment of Graphene-Based Materials: Focus on Human Health and the Environment, *ACS Nano*, 2018, **12**, 10582–10620.
55 T. L. Riss and R. A. Moravec, Comparison of MTT, XTT, and a novel Assays., tetrazolium compound for MTS for in vitro proliferation and chemosensitivity, *Mol. Biol. Cell*, 1992, **3**, 184a.